

Kapitza conductance of silicon–amorphous polyethylene interfaces by molecular dynamics simulations

Ming Hu,^{1,*} Pawel Koblinski,^{1,2,†} and Patrick K. Schelling³

¹*Rensselaer Nanotechnology Center, Rensselaer Polytechnic Institute, Troy, New York 12180, USA*

²*Department of Materials Science and Engineering, Rensselaer Polytechnic Institute, Troy, New York 12180, USA*

³*Department of Physics and Advanced Materials Processing and Analysis Center,*

University of Central Florida, Orlando, Florida 32816, USA

(Received 10 November 2008; revised manuscript received 3 February 2009; published 30 March 2009)

We use nonequilibrium molecular dynamics simulation to elucidate the interfacial thermal conductance between single-crystal silicon and amorphous polyethylene. In particular, we investigate the role of solid stiffness and the bonding strength across the interface on the interfacial thermal conductance. Simulations of interfacial scattering of individual phonon wave packets indicate that neither diffuse mismatch model nor acoustic mismatch model describes the interfacial scattering process quantitatively. In general, transmission coefficients for longitudinal phonons are significantly higher than those for transverse phonons. We also observe that anharmonic processes can be important for interfacial conductance.

DOI: [10.1103/PhysRevB.79.104305](https://doi.org/10.1103/PhysRevB.79.104305)

PACS number(s): 63.22.-m, 63.20.-e, 65.40.-b, 68.65.Cd

I. INTRODUCTION

Advances in synthesis and processing of polymer nanocomposites¹ provide opportunities in tailoring multifunctional responses of the material beyond the limits of bulk composites. Examples include simultaneous increases in strength and ductility² and very low percolation threshold for electrical transport.³ However, nanostructuring, with its associated high density of interfaces, can limit the performance of the composite. For example, the thermal conductivity of carbon nanotube (CNT)-polymer composites generally shows only modest increases over pure polymer values despite the fact that carbon nanotubes are excellent thermal conductors and with high aspect ratio. This disappointing thermal performance has been attributed to the low interfacial conductance between CNTs and a polymer matrix.⁴

The interfacial thermal conductance also known as the Kapitza conductance G_K poses a barrier to heat flow and leads to a discontinuous temperature drop ΔT across interfaces and can be quantified via the relationship⁵

$$J_Q = G_K \Delta T, \quad (1)$$

where J_Q is the heat flux across the interface. The relative importance of the interfacial conductance can be evaluated by determining the thickness of the matrix material also known as the Kapitza length l_K , over which the temperature drop is the same as at the interface. Assuming $G_K = 10^7$ W/m² K (characteristic of single-walled carbon nanotube and polymer interfaces from Ref. 6) and polymer thermal conductivity $\kappa = 0.3$ W/mK, one gets $l_K = \kappa / G_K = 30$ nm. When the separation between interfaces in nanocomposites becomes comparable to the Kapitza length l_K , interfaces will predominantly determine the overall thermal conductance. To predict the thermal properties of nanocomposites, it is therefore of critical importance to develop a deep understanding of interfacial thermal conductance.

In this paper, we report nonequilibrium molecular dynamics (MD) simulations to elucidate how G_K depends on the solid stiffness and interface bond strength for an interface

between an inorganic solid and amorphous polyethylene. A brief report of parts of this work has appeared elsewhere.⁷ However, we extend the previous study by performing wave-packet simulations of interfacial phonon scattering. The wave-packet results have led to important insights into the mechanism governing phonon transmission across polymer-solid interfaces.

The rest of the paper is organized as follows. In Secs. II A and II B, we describe the model structures and the MD methodology used to determine the thermal conductance of the interface. In Sec. III, we present and discuss the results of nonequilibrium MD simulations. In Sec. IV, we present results of MD wave-packet simulations to elucidate the mechanism governing phonon transmission at the interface. In Sec. V, we use a simple one-dimensional mass-spring model to elucidate the frequency dependence of the transmission coefficient for longitudinal-acoustic (LA) modes. Finally, the summary and conclusions are presented in Sec. VI.

II. MODEL STRUCTURES AND SIMULATION METHODOLOGY

A. Model structures

The model structure consists of two slabs: one of crystalline silicon and one of amorphous polyethylene (PE). The two slabs are in contact and are contained within a rectangular simulation box with a cross section of 21.7×21.7 Å² and a length of 133.8 Å, as shown in the top panel of Fig. 1. Periodic boundary conditions are used in all directions, resulting in two planar polymer-silicon interfaces. This geometry mimics a layered structure with silicon-polymer interfaces normal to the z direction. The silicon crystal was composed of 1696 atoms with two (100)-type surfaces. The polymer slab contained 20 chains with 40 CH₂ monomers in each chain. The initial amorphous polymer structure was generated by a method first proposed by Suter and co-workers.⁸ This method consists of a search algorithm in the space of torsion angles, which automatically delivers re-

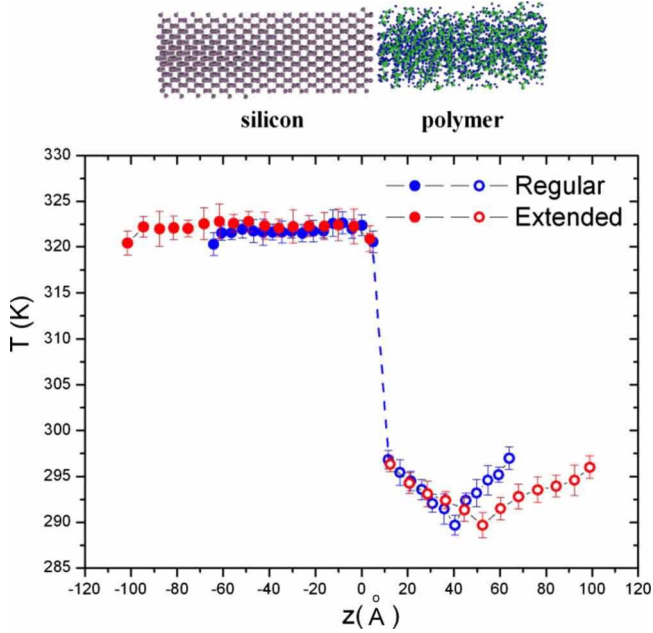


FIG. 1. (Color online) Top panel: a snapshot of model silicon-polymer interfacial structure. Bottom panel: steady-state temperature profiles for regular and extended structure. Error bars are also shown in the temperature profiles. The interfacial resistance manifests itself by a temperature drop at the interface.

alistic conformational statistics of the chains.

The interatomic interactions are described by the polymer consistent force field (PCFF) (Ref. 9) model. This PCFF force field consists of both bonded (bond stretching, bending, and torsions) and nonbonded interactions. The silicon and polymer (C and H) atoms interact by nonbonded van der Waals interactions described by the 9-6 Lennard-Jones interatomic potential $U(r) = \epsilon[2(\sigma/r)^9 - 3(\sigma/r)^6]$ with cutoff 7 Å, where r is the interatomic spacing, and the parameters ϵ and σ are energy and length scales, respectively. The parameters in interatomic potential for polymer and silicon can be found in Refs. 9 and 10, respectively. We focus on the interfacial heat transfer in this paper. In this case, the interfacial conductance is mainly determined by the speed of sound of acoustic phonons and phonon transmission coefficients. We calculated the velocities of LA and transverse-acoustic (TA) phonons in silicon from the dispersion curves using PCFF model and compared the results with experiment¹¹ and the predictions of widely used Stillinger-Weber (SW) potential.^{12,13} In particular, the group velocity of long wavelength [100] LA phonons is 8097 m/s in the PCFF model compared to 8000 m/s for the SW model and 8480 m/s in experiment. Likewise, long wavelength [100] TA phonons have a group velocity of 5465 m/s in the PCFF model compared to 5000 m/s and 5860 m/s for the SW model and experiment, respectively. These results show the PCFF model to be in excellent agreement with experiment and the SW model.

B. Simulation methodology

In the first stage of MD simulations, the system was equilibrated at a constant pressure of 1 atm and a constant

temperature of $T=300$ K for several hundred ps using integration time step of 0.5 fs. This small time step is needed due to the fact that the smallest vibrational periods associated with H atoms are of the order of 10 fs. Following equilibration, the system volume was fixed for the nonequilibrium MD simulation. The heat source was placed in the center of the silicon region and the heat sink was placed in the center of the polymer. To eliminate the tendency of the center of mass to drift as a result of velocity rescaling, we used the algorithm proposed by Jund and Jullien.¹⁴ The thermal energy delivered to heat source and removed from the heat sink at an equal rate dQ/dt . Thus, once steady state is reached, a constant heat flux $J_Q = \frac{dQ/dt}{2A}$ was established, where A is the cross-sectional area of the simulation cell. The factor of 2 accounts for the fact that with periodic boundary conditions, the heat current J_Q propagates in two directions away from the hot reservoir. The heating/cooling rate was carefully chosen through some trial runs so as the temperature drop at the interface is around 10% T , where $T=300$ K is the average temperature of the whole system. For standard force field, we found that $dQ=0.05\% k_B T$ (k_B is the Boltzmann's constant) per time step, corresponding to $J_Q=440$ MW/m², is reasonable and ensures relatively low statistical errors. By changing the direction of the heat flux, we verified that the thermal conductance is almost unchanged. However, the heat flux cannot be very large otherwise there is a rectification effect for the Si and amorphous PE system.¹⁵ In this work, the heat flux applied is in the linear-response regime so the conductance is independent of the direction of the heat flux.

To obtain temperature profiles, we divide the simulation box into slices of thickness of 4.2 Å along the z direction. The local temperature in each slice was calculated from the kinetic energies. We average the temperature profiles over 100 ps and obtain a series of about 20 temperature profiles for the whole production run of 2 ns. After 500–1000 ps, we observe that the temperature profile does not change systematically. The reported data are the steady-state averages over the last 1 ns of each production run. The temperature drop ΔT at the interface was obtained from the average temperatures of the first and the second layers of silicon and polymer near the interface. While the temperature of the first layer near the interface is slightly different from the second layer, the estimated ΔT differs by less than 5%. From the computed value of ΔT for a given heat flux J_Q , the interfacial conductance G_K can be determined using Eq. (1).

Thermal-conductivity values obtained from MD simulations can depend on the size of the simulation cell, particularly for the case of a crystalline solid, when the phonon mean-free path is comparable with the system size.¹⁶ However, our general experience is that size effects are less significant for G_K . To validate this assumption, we have in a few cases extended both silicon and polyethylene regions by 50% in heat current direction. After increasing the system size, we obtained nearly the same value G_K , as demonstrated in Fig. 1. This indicates that the size of the simulation cell is sufficient to avoid significant finite-size effects.

III. MD RESULTS AND DISCUSSION

A. Temperature profile

In the bottom panel of Fig. 1, we show typical steady-state temperature profiles for regular and extended structure

obtained with the simulation setup described above. The average temperature of the simulation cell is 300 K. The temperature profile is almost flat in the silicon region due to its large thermal conductivity. By contrast, the slope in the polymer region is fairly substantial due to the much lower conductivity of the polymer. However, the temperature drop ΔT at the silicon-polymer interface is quite large and dominates the overall thermal conductance. Since the periodic boundary conditions are used in three directions, there are two interfaces in the system. The two interfaces are independent but statistically equivalent. As a result, the two interfaces have essentially the same G_K as shown by the temperature profile in Fig. 1.

For the force field parameters in the PCFF model, we obtain the Kapitza conductance $G_K=17.4\pm 1.3$ MW/m² K for the regular structure and $G_K=17.0\pm 1.1$ MW/m² K for the extended structure. In order to further explore the possibility of finite-size effects, we also simulated a diamondlike solid/PE interface at room temperature and also the Si-PE interface at 200 K. We found in both of these cases that the results for the regular and extended systems were identical within the computed statistical error. This further establishes that finite-size effects play a very little role in determining G_K .

From separate simulations of the thermal conductivity of bulk PE, we determined that the thermal conductivity of the polymer is about 0.33 W/mK. From these results, we obtain a Kapitza length $l_K=19$ nm. In other words, the interface possesses the equivalent resistance of a 19-nm-thick PE film. This interfacial conductance is in the range 10–40 MW/m² K that contains the Kapitza conductance between the carbon nanotube,⁴ diamond,¹⁷ oxides (e.g., alumina¹⁸), and organic materials.

B. Effect of solid stiffness

The dependence of G_K on the solid stiffness of the crystalline solid is shown in Fig. 2. Here, we increased the spring constants representing covalent bonds, bond-bending terms, and torsional terms by factors of 2, 4, and 8 from the values that are characteristic of silicon. This translates into range of elastic modulus of 100–1000 GPa. The lower limit corresponds to silicon, while the upper limit is comparable to diamond.

We find that as the modulus of the solid increases, G_K decreases. This behavior is expected since the mismatch between vibrational modes of the soft polymer and the solid increases as the stiffness of the solid increases. By making a power-law fit (see dotted line in Fig. 2), we found $G\sim E^\alpha$ with $\alpha\approx -0.36$. This power-law dependence is rather weak and, as shown in Fig. 2, the interfacial conductance only decreases by half for the modulus of 1000 GPa.

In Fig. 2 we also compare the thermal conductance obtained in our simulations with the predictions of a number of models, including acoustic mismatch model (AMM), diffuse mismatch model (DMM), and phonon radiation limit (PRL).^{5,19–21} PRL represents the maximum possible conductance by assuming a transmission coefficient of unity for all phonons in silicon with frequencies below the highest-

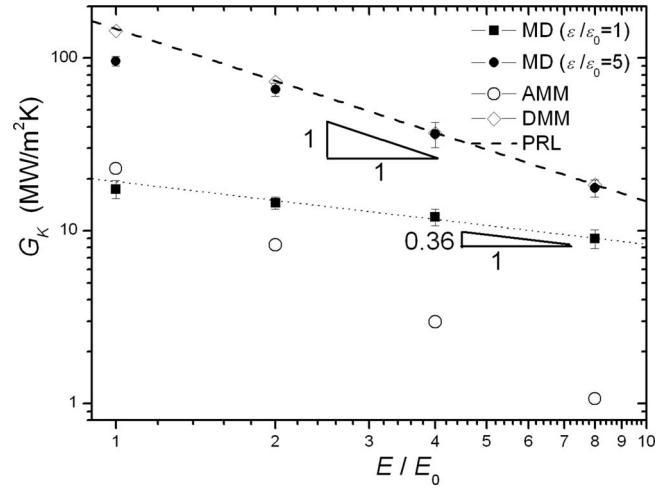


FIG. 2. Silicon-polymer interfacial thermal conductance as a function of solid modulus normalized by E_0 . E_0 is modulus of silicon with the standard force field and E is the Young's modulus of modified silicon. ϵ_0 is the standard van der Waals interaction strength between silicon and polymer atoms. ϵ is modified interaction strength. The dotted line is a power-law fit to the data. The dashed line with a slope of -1 represents the PRL prediction of the thermal conductance. The predictions of AMM and DMMs are also included.

frequency vibrational mode of polyethylene ν_{\max} and a transmission coefficient of zero for phonons in silicon with frequencies greater than ν_{\max} . The radiation limit is, therefore, a function of the cut-off vibrational frequency ν_{\max} of polyethylene and the Debye density of states in silicon.²¹ In our calculation, we used the longitudinal and transverse speed of sound in Si and c_l and c_t obtained from PCFF model equal to 8097 and 5465 m/s, respectively. When we increase the spring constants up to the diamond case, we account for the changes in the speed of sound via its proportionality to the square root of solid modulus.

The maximum frequency ν_{\max} is taken as 5 THz estimated from vibrational spectra in silicon and polyethylene, as shown in Fig. 3. The vibrational spectra presented in Fig. 3 were calculated for carbon atoms in PE and Si atoms in crystalline slab via a Fourier transform of the atomic velocity autocorrelation function.^{22,23} For the radiation limit model, we estimate the cut-off vibrational frequency ν_{\max} as 5 THz because at this point the vibration spectra intensity in PE is decaying to a small value. As we will see from our phonon-scattering study beyond 5 THz, transmission coefficients for phonons are rather small (see Sec. IV for details).

For the case considered here, the DMM displays essentially the same behavior as the PRL (see open diamonds and dashed line in Fig. 2). In the DMM, phonons are transmitted or reflected with probability proportional to the density of vibrational states on either side of the interface. Below ν_{\max} , the phonon density of states is much higher in the PE than in the Si. As a result, the transmission coefficient for phonons incident from the Si with frequencies below ν_{\max} is close to unity. This is exactly the same assumption made for the PRL. In contrast to the DMM, the AMM predicts much lower interfacial conductance (see open circles in Fig. 2). This origi-

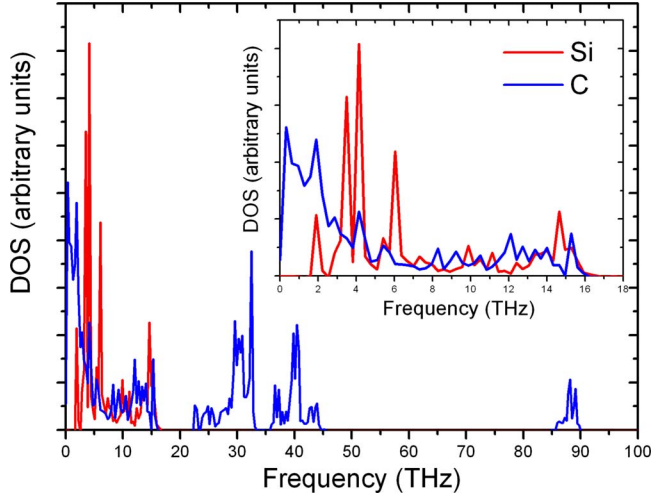


FIG. 3. (Color online) Vibrational spectra intensity of silicon and carbon atoms in polyethylene computed from the Fourier transforms of the velocity autocorrelation function. The discrete nature of the computed spectra results from the finite size of the simulation cell. Inset: the low-frequency portion of the spectrum where there is substantial overlap between Si and polyethylene.

nates from the fact that the phonon transmission in the AMM is governed by the mismatch in the acoustic impedance, which is very large for the interface between the crystalline solid and the amorphous PE. In particular, mainly due to the large difference in the modulus, the acoustic impedance for the crystal has a range between 1.74×10^8 and 1.39×10^9 kg/m² s whereas the acoustic impedance for the PE is about 8.77×10^5 kg/m² s. Consequently, the transmission coefficients predicted by the AMM are much smaller than unity (around 0.15). In both the AMM and DMM, the exact nature of the interfacial bonds is not taken into consideration.

As discussed above, with regular Si-PE force field parameters, the interfacial conductance is between the prediction of DMM and AMM and depends weakly on solid modulus. By contrast, increasing the strength of the Si-PE interactions by a factor of 5 significantly increases G_K to values in close agreement with the predictions of the DMM (see solid circles in Fig. 2). This may lead to a speculation that with a strong interfacial bonding, heat transfer across polymer-inorganic solid interface is well described by the DMM. However, direct phonon-scattering studies described in Sec. IV indicate that this is not the case. With weaker bonding the mechanism of phonon transmission is also not clear and perhaps changes with increasing solid stiffness. In Sec. IV, we will further address these issues by analyzing the results of wave-packet simulations.

C. Effect of temperature

To explore the possibility that anharmonic phonon scattering affects G_K , we computed G_K as a function of temperature in the range of 200–400 K. In a similar study, Stevens *et al.*²⁴ found by using the nonequilibrium MD simulation that G_K at solid-solid interfaces strongly increased with increasing temperature. Likewise, the results presented in Fig. 4 show a

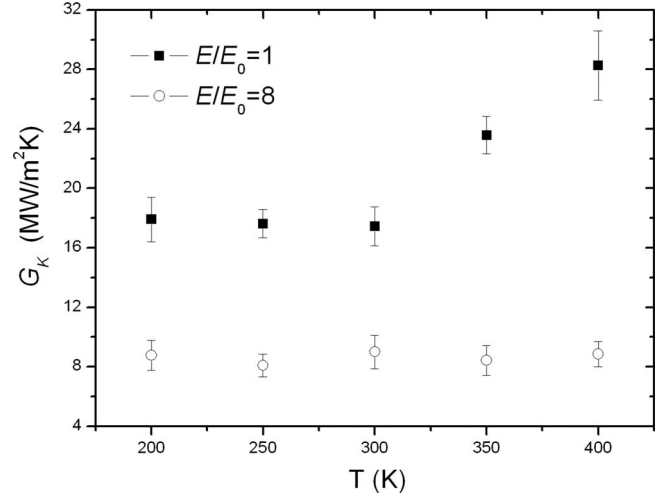


FIG. 4. Silicon-polymer (solid squares) and “diamond-polymer” (open circles) interfacial thermal conductance plotted as a function of temperature.

strong temperature dependence above $T=300$ K for $E/E_0=1$ corresponding to ordinary Si. By contrast, for $E/E_0=8$, corresponding approximately to diamond, G_K is temperature independent in the same temperature range, indicative of purely harmonic processes. These results indicate that anharmonic processes can under some circumstances play an important role in G_K . However, contrary to what might be expected, anharmonic effects within the bulk of the crystalline slab seem to be important for G_K . This observation is consistent with a recent article by Aubry *et al.*²⁵ that demonstrated how computed values of G_K depend on the nature of scattering in the bulk. We have not determined how changing the bonding strength between the crystalline solid and the PE affects the temperature dependence of G_K .

D. Effect of interfacial bonding strength

While the temperature dependence of G_K is moderate, the interfacial bonding strength dependence is very strong, as shown in Fig. 5. As the interfacial bond strength is increased up to $\epsilon/\epsilon_0=5$, G_K increases more or less linearly. At $\epsilon/\epsilon_0=5$, G_K is 96 ± 6.1 MW/m² K, which is about six times larger than the value for $\epsilon/\epsilon_0=1$, which is 17 ± 1.3 MW/m² K. By contrast, G_K is nearly independent of ϵ/ϵ_0 for values above about 5.

This behavior can be understood qualitatively in terms of the Si-polymer bond playing intermediately between soft polymer-polymer bonds and stiff Si-Si bonds. This creates a “graded interface.” Such interfaces lead to higher phonon transmission provided that the strength of the interfacial bond is between the strength of the bonds present in the two materials forming the interface. As has been reported, e.g., in Refs. 26–28, the phonon transmission across graded interfaces is better than across abrupt interfaces (see also Sec. V for more discussion).

IV. WAVE-PACKET SIMULATION RESULTS

To understand the underlying transport mechanisms at the interface, we performed phonon wave-packet simulations.²⁹

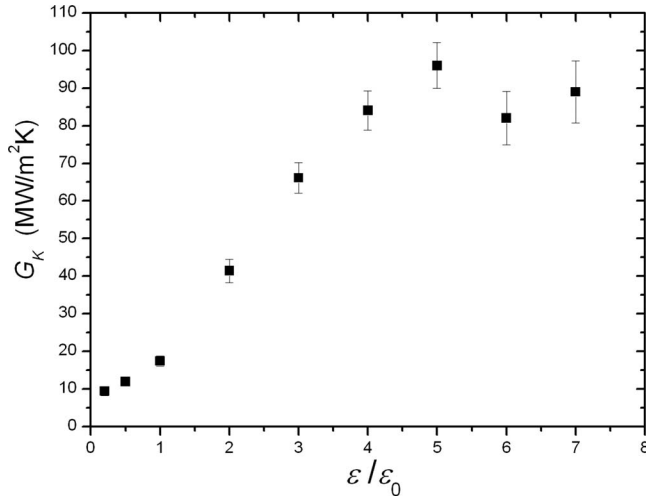


FIG. 5. Silicon-polymer interfacial thermal conductance as a function of interfacial bonding strength.

In this case the simulation cell consists of a $3 \times 3 \times 201$ Si slab, which is about 1100 Å long in the z direction and a 210 Å long amorphous PE slab. The whole structure is first relaxed to the zero-temperature configuration. Then a vibrational wave packet with a well-defined wave vector and polarization is introduced in the silicon slab. The phonon wave packets are formed from linear combinations of vibrational eigenstates. The eigenstates themselves are found by diagonalizing the dynamical matrix of the perfect crystal. To generate a wave packet centered at a wave vector \mathbf{k}_0 in band λ , we displace the atoms according to²⁹

$$u_{i\mu} = A_m \phi_{i\mu\lambda}(\mathbf{k}_0) \exp[i\mathbf{k}_0 \cdot (z_l - z_0)] \exp[-\eta^2(z_l - z_0)^2], \quad (2)$$

where $u_{i\mu}$ is the μ th ($\mu=1, 2, 3$) component of displacement for atom i in the unit cell labeled by l , A_m is the amplitude of the wave, $\phi_{i\mu\lambda}$ is the polarization vector for band λ at \mathbf{k}_0 , z_0 is the space coordinates where we desire the wave packet to be around, and $1/\eta$ is the spatial extent of the wave packet. An initial displacement field of a representative wave packet is presented in Fig. 6(a). When the wave packet is launched, it propagates toward the interface. After arriving at the interface, part of the energy is transmitted and the remainder is reflected [Figs. 6(b) and 6(c)]. The energy-transmission coefficient is determined from the ratio of the transmitted to the incident energy.

Figure 6 shows a series of snapshots of the atomic displacements for an incident LA wave packet with average frequency $f=1.47$ THz. For the case with $\varepsilon/\varepsilon_0=1$ most of the incident energy is reflected from the interface [see Fig. 6(b)] with energy-transmission coefficient $\alpha=0.13$, while for the case with $\varepsilon/\varepsilon_0=5$ a larger fraction of the energy in the incident LA mode is transmitted into polymer with $\alpha=0.33$. It is worth noticing that apart from the low-frequency limit, there are no ballistically propagating phonons in PE as its structure is amorphous. By analyzing the frequency of silicon and PE on both sides of the interface, we found that the frequency is mostly preserved once the part of the phonon

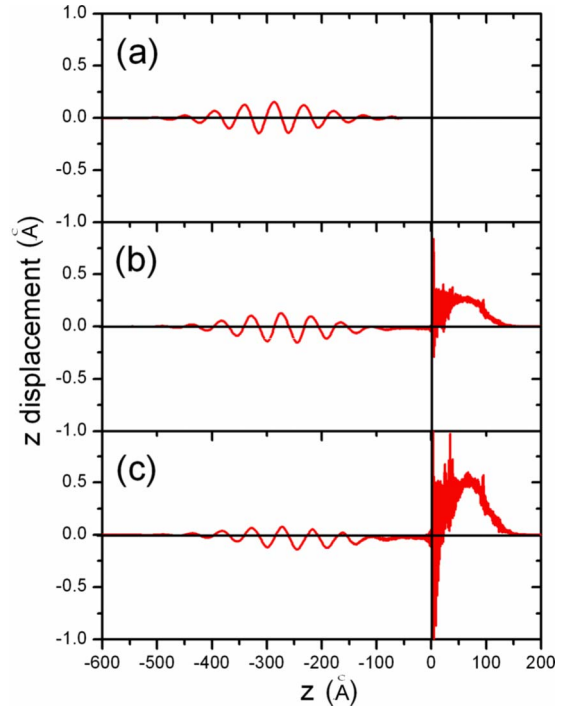


FIG. 6. (Color online) Snapshots of displacements for an LA wave packet with $f=1.47$ THz (a) before scattering, (b) after scattering $\varepsilon/\varepsilon_0=1$, and (c) after scattering $\varepsilon/\varepsilon_0=5$.

energy crosses the interface. This can be attributed to the fact that the phonon modes in PE is very abundant across almost the whole frequency range in silicon, especially in the range of low and intermediate frequencies we studied in wave-packet dynamics simulation (see Fig. 3).

Figure 7 shows the frequency-dependent energy-transmission coefficients for incident LA and TA wave packets. With $\varepsilon/\varepsilon_0=1$, the transmission coefficient α is only appreciable at low frequencies but never is greater than about 0.35. Furthermore, α for LA modes is larger than those of the TA modes across the whole frequency range. This is likely

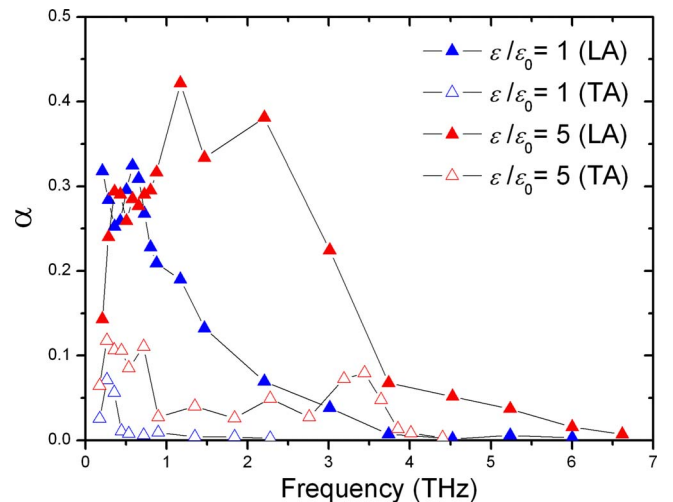


FIG. 7. (Color online) Frequency dependence of the energy-transmission coefficient.

associated with the fact that atomic displacements for LA modes are normal to the interface, while displacements for TA modes are parallel to the interface.

When the interfacial bonding strength is increased to $\varepsilon/\varepsilon_0=5$, the transmission coefficient of both incident LA and TA modes becomes much higher in the 1–4 THz frequency range and this is the main reason that the increasing interaction strength leads to increased interfacial conductance. Interestingly, with strong interactions, the computed α reaches an apparent maximum of about 0.42 in the frequency range between 1 and 2 THz.

We note that the acoustic mismatch model predicts the transmission coefficient of about 0.15 for our model and the diffuse mismatch model predicts the transmission coefficient close to unity. In the low-frequency range, LA modes even with weak interfacial interactions have larger transmission coefficient than that predicted by the AMM and significantly lower than that predicted by DMM. However, the data indicate that neither AMM nor DMM is capable of quantitative description of the scattering process.

To make a connection between the interfacial conductance and transmission coefficients estimate, we note that G_K can be estimated as being proportional to $\int_0^{\nu^{\max}} \alpha(\nu) \nu^2 d\nu$, where ν^2 is due to phonon density of states characterizing the Debye model of solid. A more complete expression includes the phonon group velocity, however, we will assume that it is equal to the speed of sound. This integral can be performed for the cases of weak and strong interfacial bonds $\varepsilon/\varepsilon_0=1$ and $\varepsilon/\varepsilon_0=5$, respectively. The ratio of this integral for the two cases predicts an increase in G_K by a factor of 6.6 when the bond strength is increased. This result is in good agreement with the increase in G_K predicted by direct MD simulation (see Fig. 5).

V. ONE-DIMENSIONAL CHAIN MODEL ANALYSIS

To provide a simple qualitative picture of the origin of frequency dependence of the transmission coefficient for LA modes on the bonding strength, we consider a one-dimensional chain model of masses connected by linear springs. In one half of the infinite chain, the mass, spring length, and spring constant were adjusted so as to reproduce the LA branch dispersion as well as acoustic impedance for Si. Analogously, in the other half, the chain represents acoustic PE properties. The bond between Si and PE is treated as an adjustable parameter.

We calculated the transmission coefficient as a function of frequency using the Green's function formalism and Caroli formula.^{30–32} For this simple model, the following analytical solution of transmission coefficients yields:

$$\alpha(\omega) = 4k_{\text{Si-PE}}^2 k_{\text{Si-Si}} k_{\text{PE-PE}} \sin(q) \sin(q') / |d|^2, \quad (3)$$

where $k_{\text{Si-Si}}$, $k_{\text{PE-PE}}$, and $k_{\text{Si-PE}}$ are the stiffness of the springs connecting Si-Si, PE-PE, and Si-PE masses, respectively, $d = [\omega^2 - k_{\text{Si-PE}} + k_{\text{Si-Si}}(e^{iq} - 1)][\omega^2 - k_{\text{Si-PE}} + k_{\text{PE-PE}}(e^{iq'} - 1)]$ is the determinant of the Green's function of the one-dimensional chain model, and q and q' are the wave numbers of Si and PE chains, respectively. Then we adjusted the value of the spring constant that connects Si and PE chains to best fit the

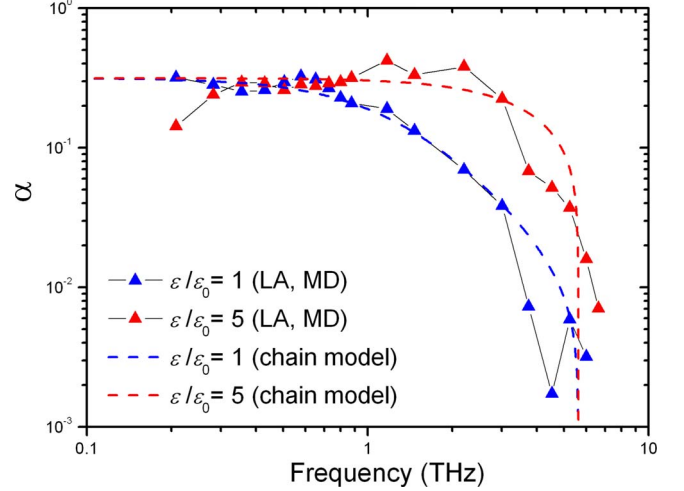


FIG. 8. (Color online) Frequency-dependent energy-transmission coefficient fitted by a one-dimensional chain model.

data obtained by phonon-scattering MD simulations. The results of fits to the wave-packet simulations with $\varepsilon/\varepsilon_0=1$ and $\varepsilon/\varepsilon_0=5$ are shown in Fig. 8. The best fit for $\varepsilon/\varepsilon_0=1$ was obtained with $k_{\text{Si-PE}}/k_{\text{Si-Si}}=0.008$. This low value of $k_{\text{Si-PE}}/k_{\text{Si-Si}}$ is understandable since there are no covalent bonds between Si and PE. We also note that the fit for $\varepsilon/\varepsilon_0=1$ is quite good almost across the whole frequency range indicating that the mechanism of LA phonon scattering between PE and Si with normal bonding strength is well described by the chain model.

The best fit for $\varepsilon/\varepsilon_0=5$ was obtained for $k_{\text{Si-PE}}/k_{\text{Si-Si}}=0.025$, which is consistent with the fact that the bonding strength between PE and Si is larger in this case.

We can also use the one-dimensional chain model to determine the transmission coefficients as a function of interfacial bonding strength. The results are shown in Fig. 9 for an incident LA mode with frequency 2 THz. As the spring stiff-

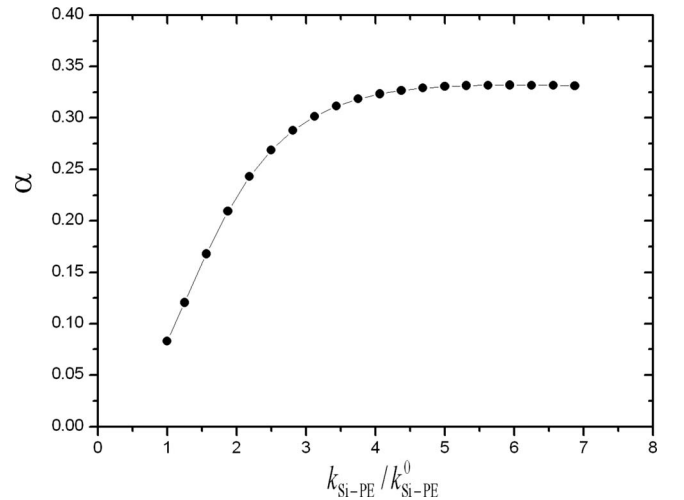


FIG. 9. For the one-dimensional chain model; dependence of the energy-transmission coefficient on the interfacial bond strength for incident waves with a frequency of 2 THz. $k_{\text{Si-PE}}^0$ is the stiffness of the spring connecting Si-PE which is best fitted for the case of $\varepsilon/\varepsilon_0=1$. $k_{\text{Si-PE}}$ is the modified bond strength at the interface.

ness is increased by a factor of 5, the transmission coefficient increases by a factor of 4. However, further increases do not significantly change the value of α . Figure 9 has nearly the same trends as Fig. 5, which indicates that the mechanism of LA phonon scattering between PE and Si with both normal and strong bonding strength can be described by the one-dimensional chain model.

VI. SUMMARY AND CONCLUSION

Investigations of the interfacial thermal conductance between single-crystal silicon and amorphous polyethylene have been presented.

Using nonequilibrium molecular dynamics simulations, we have studied the dependence of the interfacial thermal conductance as a function of solid modulus and interfacial bonding. We found that as the modulus of the solid increases by a factor of 8, the interfacial conductance decreases only by half. By contrast, a fivefold increase in the interfacial bonding strength leads to about a fivefold increase in the interfacial conductance. This suggests that tailoring the soft-hard interfaces for better thermal transport should focus on development of stronger interfacial bonds rather than softening of the solid. This could be done in practice for some polymer-solid interfaces where, in addition to van der Waals

interactions, stronger dipolar or Coulomb interaction might be present.

The wave-packet simulation of individual phonon scattering provided us with insights into the mechanism governing phonon transmission across polymer-solid interfaces. We found that the significant transmission is only observed up to about 5 THz, i.e., within the range of soft modes motion in PE. The increasing interfacial bonding leads to an increase in the transmission coefficients in the 1–4 THz frequency range, which is responsible for the overall increase in the interfacial conductance. Furthermore, the transmission coefficients for longitudinal phonons are generally significantly higher than those for transverse phonons. In general, neither acoustic mismatch model nor diffuse mismatch model is capable of quantitatively predicting scattering coefficient.

Finally, we used a simple one-dimensional chain model of masses connected by linear springs to further elucidate the origin of frequency and dependence of the transmission coefficient. We found that qualitatively the frequency dependence of the transmission coefficient for longitudinal-acoustic phonons is described well by the chain model for both strongly and weakly bonded interfaces.

ACKNOWLEDGMENTS

This work was supported by the AFOSR/MURI program under Grant No. FA9550-08-1-0407.

*Corresponding authors; hum@ethz.ch

†keblip@rpi.edu

¹K. I. Winey and R. A. Vaia, *MRS Bull.* **32**, 314 (2007).

²P. C. LeBaron, Z. Wang, and T. J. Pinnavaia, *Appl. Clay Sci.* **15**, 11 (1999).

³F. M. Du, R. C. Scogna, W. Zhou, S. Brand, J. E. Fischer, and K. I. Winey, *Macromolecules* **37**, 9048 (2004).

⁴S. Shenogin, L. P. Xue, R. Ozisik, P. Keblinski, and D. G. Cahill, *J. Appl. Phys.* **95**, 8136 (2004).

⁵E. T. Swartz and R. O. Pohl, *Rev. Mod. Phys.* **61**, 605 (1989).

⁶S. T. Huxtable, D. G. Cahill, S. Shenogin, L. P. Xue, R. Ozisik, P. Barone, M. Usrey, M. S. Strano, G. Siddons, M. Shim, and P. Keblinski, *Nature Mater.* **2**, 731 (2003).

⁷M. Hu, S. Shenogin, and P. Keblinski, *Appl. Phys. Lett.* **91**, 241910 (2007).

⁸M. Müller, J. Nievergelt, S. Santos, and U. W. Suter, *J. Chem. Phys.* **114**, 9764 (2001).

⁹H. Sun, S. J. Mumby, J. R. Maple, and A. T. Hagler, *J. Am. Chem. Soc.* **116**, 2978 (1994).

¹⁰H. Sun, *Macromolecules* **28**, 701 (1995).

¹¹M. G. Holland, *Phys. Rev.* **132**, 2461 (1963).

¹²F. H. Stillinger and T. A. Weber, *Phys. Rev. B* **31**, 5262 (1985).

¹³P. K. Schelling and S. R. Phillpot, *J. Appl. Phys.* **93**, 5377 (2003).

¹⁴P. Jund and R. Jullien, *Phys. Rev. B* **59**, 13707 (1999).

¹⁵M. Hu, P. Keblinski, and B. W. Li, *Appl. Phys. Lett.* **92**, 211908 (2008).

¹⁶P. K. Schelling, S. R. Phillpot, and P. Keblinski, *Phys. Rev. B* **65**, 144306 (2002).

¹⁷C. K. Leong and D. D. L. Chung, *Carbon* **41**, 2459 (2003).

¹⁸A. Devpura, P. E. Phelan, and R. S. Prasher, *Microscale Thermophys. Eng.* **5**, 177 (2001).

¹⁹N. S. Snyder, *Cryogenics* **10**, 89 (1970).

²⁰R. J. Stoner and H. J. Maris, *Phys. Rev. B* **48**, 16373 (1993).

²¹H. K. Lyeo and D. G. Cahill, *Phys. Rev. B* **73**, 144301 (2006).

²²L. V. Zhigilei, D. Srivastava, and B. J. Garrison, *Surf. Sci.* **374**, 333 (1997).

²³S. R. Calvo and P. B. Balbuena, *Surf. Sci.* **581**, 213 (2005).

²⁴R. J. Stevens, L. V. Zhigilei, and P. M. Norris, *Int. J. Heat Mass Transfer* **50**, 3977 (2007).

²⁵S. Aubry, C. J. Kimmer, A. Skye, and P. K. Schelling, *Phys. Rev. B* **78**, 064112 (2008).

²⁶K. Jagannadham, *J. Vac. Sci. Technol. A* **17**, 373 (1999).

²⁷K. Jagannadham and H. Wang, *J. Appl. Phys.* **91**, 1224 (2002).

²⁸K. J. Wang, Q. G. Guo, G. B. Zhang, J. L. Shi, and L. Liu, *Surf. Coat. Technol.* **201**, 7472 (2007).

²⁹P. K. Schelling, S. R. Phillpot, and P. Keblinski, *Appl. Phys. Lett.* **80**, 2484 (2002).

³⁰C. Caroli, R. Combescot, P. Nozieres, and D. Saint-James, *J. Phys. C* **4**, 916 (1971).

³¹J. S. Wang, J. Wang, and N. Zeng, *Phys. Rev. B* **74**, 033408 (2006).

³²J. S. Wang, N. Zeng, J. Wang, and C. K. Gan, *Phys. Rev. E* **75**, 061128 (2007).